Supernova 2012ec: identification of the progenitor and early monitoring with PESSTO[★]

J. R. Maund,[1,2][†][‡] M. Fraser,[1] S. J. Smartt,[1] M. T. Botticella,[3] C. Barbarino,[3]
M. Childress,[4] A. Gal-Yam,[5] C. Inserra,[1] G. Pignata,[6] D. Reichart,[7] B. Schmidt,[4]
J. Sollerman,[8] F. Taddia,[8] L. Tomasella,[9] S. Valenti[10,11] and O. Yaron[5]

[1]*Astrophysics Research Centre, School of Mathematics and Physics, Queen's University Belfast, Belfast BT7 1NN, UK*
[2]*Dark Cosmology Centre, Niels Bohr Institute, University of Copenhagen, Juliane Maries Vej 30, DK-2100 Copenhagen, Denmark*
[3]*INAF – Osservatorio astronomico di Capodimonte, Salita Moiariello 16, I-80131 Napoli, Italy*
[4]*Research School of Astronomy and Astrophysics, Australian National University, Cotter Road, Weston Creek, ACT 2611, Australia*
[5]*Department of Particle Physics and Astrophysics, The Weizmann Institute of Science, Rehovot 76100, Israel*
[6]*Departamento de Ciencias Fisicas, Universidad Andres Bello, Avda. Republica 252, Santiago, Chile*
[7]*Department of Physics and Astronomy, University of North Carolina at Chapel Hill, 120 E. Cameron Ave., Chapel Hill, NC 27599, USA*
[8]*The Oskar Klein Centre, Department of Astronomy, AlbaNova, Stockholm University, SE-10691 Stockholm, Sweden*
[9]*INAF – Osservatorio Astronomico di Padova, Vicolo dell'Osservatorio 5, I-35122 Padova, Italy*
[10]*Las Cumbres Observatory Global Telescope Network, 6740 Cortona Dr., Suite 102, Goleta, CA 93117, USA*
[11]*Department of Physics, University of California, Santa Barbara, Broida Hall, Mail Code 9530, Santa Barbara, CA 93106-9530, USA*

ABSTRACT

We present the identification of the progenitor of the Type IIP SN 2012ec in archival pre-explosion *Hubble Space Telescope* Wide Field Planetary Camera 2 (WFPC2) and Advanced Camera for Surveys Wide Field Channel *F814W* images. The properties of the progenitor are further constrained by non-detections in pre-explosion WFPC2 *F450W* and *F606W* images. We report a series of early photometric and spectroscopic observations of SN 2012ec. The r'-band light curve shows a plateau with $M_{r'} = -17.0$. The early spectrum is similar to the Type IIP SN 1999em, with the expansion velocity measured at Hα absorption minimum of $-11\,700\,\mathrm{km\,s^{-1}}$ (at 1 d post-discovery). The photometric and spectroscopic evolution of SN 2012ec shows it to be a Type IIP SN, discovered only a few days post-explosion (<6 d). We derive a luminosity for the progenitor, in comparison with MARCS model spectral energy distributions, of $\log L/\mathrm{L_\odot} = 5.15 \pm 0.19$, from which we infer an initial mass range of 14–22 $\mathrm{M_\odot}$. This is the first SN with an identified progenitor to be followed by the Public ESO Spectroscopic Survey of Transient Objects (PESSTO).

Key words: supernovae: general – supernovae: individual: 2012ec – galaxies: individual: NGC 1084.

1 INTRODUCTION

The hydrogen-rich Type IIP supernovae (SNe) are the most common type of SN in the local universe (Cappellaro & Turatto 2001; Li et al. 2011). The standard prediction of stellar evolution models is that such SNe arise from the lowest mass stars to end their lives as core-collapse (CC) SNe, whilst still retaining their massive hydrogen envelopes that give rise to the characteristic light-curve plateau (Heger et al. 2003; Eldridge & Tout 2004). Red supergiants have been directly observed at the sites of these SNe in fortuitous pre-explosion images (see Smartt 2009, for a review) and, with the observation of the disappearance of the progenitor stars in late-time post-explosion images, this scenario for the production of Type IIP SNe has been confirmed (Maund & Smartt 2009). A number of key problems are still outstanding in our understanding of Type IIP SNe, in particular the diversity in the explosion energies and the amounts of ^{56}Ni produced in these events (Pastorello et al. 2006), and the apparent deficit of observed progenitors with $M_{\mathrm{ZAMS}} \gtrsim 16\,\mathrm{M_\odot}$ (termed the 'Red Supergiant Problem'; Smartt et al. 2009).

We report the identification of the progenitor of the Type IIP SN 2012ec in pre-explosion *Hubble Space Telescope (HST)* Wide Field Planetary Camera 2 (WFPC2) and Advanced Camera for Surveys
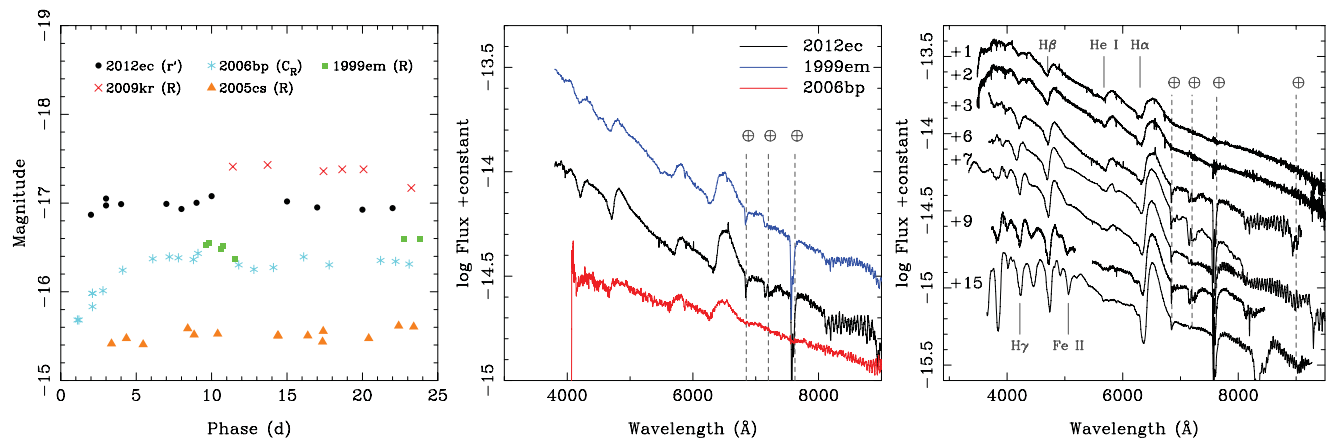
Figure 1. The early photometric and spectroscopic characteristics of the Type IIP SN 2012ec. Left-hand panel: early r' photometry of SN 2012ec compared to other Type II SNe: 2009kr (Fraser et al. 2010), 2006bp (Quimby et al. 2007), 2005cs (Pastorello et al. 2006) and 1999em (Hamuy et al. 2001; Elmhamdi et al. 2003). The phase of the SN 2012ec data is given with respect to the date of discovery. Centre panel: the early spectrum of SN 2012ec compared to the normal Type IIP SNe 1999em (Hamuy et al. 2001; Elmhamdi et al. 2003) and 2006bp (Quimby et al. 2007), at +7 and 9 d post-explosion, respectively (the SN spectra have been corrected for the respective recessional velocities of their host galaxies and for foreground Milky Way extinction, as quoted by NED). Right-hand panel: the early spectroscopic evolution of SN 2012ec, with the phase of each spectrum given relative to the date of discovery (2012 August 11). Characteristic lines, observed in the spectra of Type IIP SNe, are indicated by the solid grey lines, and telluric features are indicated by the dashed grey lines.

(ACS) images, and the early photometric and spectroscopic properties of the SN. SN 2012ec was discovered by Monard (2012) on 2012 August 11.039 UT. The SN is located 0.7 arcsec E and 15.9 arcsec N of the centre of the host galaxy NGC 1084. A spectrum of the SN acquired on 2012 August 12 showed it to be a young Type IIP SN, a few days post-explosion (Childress et al. 2012). NGC 1084 has previously hosted four SNe: 2009H (Li, Cenko & Filippenko 2009), 1998dl (King et al. 1998), 1996an (Nakano et al. 1996) and 1963P.

The Tully–Fisher distance (Tully et al. 2008), quoted from the Extragalactic Distance Database,[1] is $\mu = 31.19 \pm 0.13$ mag. The position of SN 2012ec is coincident with the region C9 identified by Ramya, Sahu & Prabhu (2007) in NGC 1084, for which they derive an oxygen abundance of $12 + \log\left(\frac{O}{H}\right) = 8.93 \pm 0.1$. Assuming a solar metallicity corresponding to an oxygen abundance of 8.66 ± 0.05 (Asplund et al. 2004), we adopt a metallicity of $\log\left(Z/Z_\odot\right) \approx +0.27$ at the position of the SN. The degree of foreground Galactic reddening is $E(B - V) = 0.024$ mag (Schlafly & Finkbeiner 2011).[2]

2 THE EARLY PHOTOMETRIC AND SPECTROSCOPIC CHARACTERISTICS OF SN 2012EC

A photometric and spectroscopic campaign to follow the evolution of this SN is being conducted by the Public ESO Spectroscopic Survey of Transient Objects (PESSTO) collaboration.[3] Full results of the observations of this SN will be presented in a future Letter; here we present a subset of these observations to classify and characterize the early time behaviour of SN 2012ec. Photometry was collected using the Panchromatic Robotic Optical Monitoring and Polarimetry telescopes (Reichart et al. 2005) and the Liverpool Telescope using RATcam and the Infrared Optical camera. The photometric observations were conducted using Sloan filters, and were reduced

in the standard fashion using IRAF[4] and calibrated against stars in the Sloan DR6 catalogue.[5] The r'-band light curve (in the Vega magnitude system) is presented in Fig. 1 and compared with light curves of other Type II SNe in similar, but *not identical*, bands. The light curve of SN 2012ec clearly shows a plateau, implying that the SN is a Type IIP SN. The absolute magnitude (corrected for the distance and foreground and host extinction; see below) of SN 2012ec, on the plateau, is $M_{r'} = -17.0 \pm 0.1$ mag, which is slightly brighter than normal Type IIP SNe in terms of $\sim R$-band brightness (Arcavi et al. 2012), but it is clearly brighter than the subluminous SN 2005cs (Pastorello et al. 2006).

Spectroscopic observations were conducted with a number of telescopes and instruments: at 1 and 2 d (post-discovery) using the Australian National University 2.3 m telescope and the Wide Field Spectrograph integral field spectrograph (Dopita et al. 2007), using the B3000/R3000 grism (previously presented by Childress et al. 2012); at 3 d using the Nordic Optical Telescope using the Andalucia Faint Object Spectrograph and Camera and the Gr#4 grism; at 6 d with the Asiago 1.8 m telescope using *Asiago* Faint Object Spectrograph and Camera and the Gr#4; at 7 and 15 d with the New Technology Telescope using ESO Faint Object Spectrograph and Camera 2 and grisms Gr#11 and Gr#16 for the first epoch, and the Gr#13 grism for the second epoch; and at 9 d with the William Herschel Telescope using the Intermediate dispersion Spectrograph and Imaging System and R300B and R158R grisms. The sequence of spectroscopic observations is shown on Fig. 1. The spectra presented in this Letter are available in electronic format on the Weizmann interactive supernova data repository (WISeREP; Yaron & Gal-Yam 2012[6]). At early times the spectrum of SN 2012ec is similar to spectra of Type IIP SNe, being dominated by broad P Cygni profiles associated with the hydrogen Balmer series. Fits

---

[1] http://edd.ifa.hawaii.edu/
[2] Quoted from NED http://ned.ipac.caltech.edu.
[3] http://www.pessto.org

[4] IRAF is distributed by the National Optical Astronomy Observatory, which is operated by the Association of Universities for Research in Astronomy (AURA) under cooperative agreement with the National Science Foundation.

[5] http://www.sdss.org/dr6/
[6] http://www.weizmann.ac.il/astrophysics/wiserep

Table 1. High spatial resolution observations of the site of SN 2012ec.

Date	Instrument	Filter	Exposure time (s)
2001 Nov 6	*HST*/WFPC2/PC	*F450W*	320
2001 Nov 6	*HST*/WFPC2/PC	*F606W*	320
2001 Nov 6	*HST*/WFPC2/PC	*F814W*	320
2010 Sep 20	*HST*/ACS/WFC	*F814W*	1000
2012 Aug 14	VLT/NACO	K_S	780

conducted using GELATO (Harutyunyan et al. 2008)[7] identified similarities between the first spectrum of SN 2012ec and the spectrum of SN 1999em at ∼7 d post-explosion (Elmhamdi et al. 2003) and earlier for other examples of Type IIP SNe, suggesting SN 2012ec was discovered <6 d post-explosion. At the first epoch, the velocity at the Hα absorption minimum was measured to be −11 700 km s^{-1}. Over the sequence of spectra, the velocity of Hα decreased to −9200 km s^{-1} 15 d post-discovery. The Hα velocity, and its evolution, is similar to that observed for SN 1999em (Hamuy et al. 2001) and SN 2006bp (between 6 and 8 d post-explosion; Quimby et al. 2007). The velocities are significantly faster (by ∼4300 km s^{-1}), and the rate of decline is slower, than observed for SN 2005cs at early times (Pastorello et al. 2009).

The unresolved Na I D doublet is observed in absorption at the recessional velocity of NGC 1084 at all epochs. We measure an average equivalent width $W_{\mathrm{Na I D}} = 0.72 \pm 0.3$ Å. Assuming Galactic-type dust, this equivalent width corresponds to $E(B - V) = 0.11$ mag (Turatto, Benetti & Cappellaro 2003) or $E(B - V) = 0.10^{+0.15}_{-0.02}$ mag (Poznanski, Prochaska & Bloom 2012), and we adopt the latter for the total reddening towards SN 2012ec (for identical Galactic and host reddening laws; Cardelli, Clayton & Mathis 1989).

3 PROGENITOR OBSERVATIONS AND ANALYSIS

3.1 Observations

The pre- and post-explosion high spatial resolution observations of the site of SN 2012ec are listed in Table 1. Adaptive optics observations were acquired with the Very Large Telescope/Nasmyth Adaptive Optics System (NAOS) and the CONICA camera (VLT/NACO) instrument on 2012 August 14. The observations were composed of dithered on-target exposures, interleaved with offset sky images to aid with the removal of the sky background, with the K_S-band filter. The data were reduced using the ECLIPSE package.[8] The observations used the S54 camera (with pixel scale 0.0543 arcsec) and, under the observing conditions, a full width at half-maximum of 0.13 arcsec, and Strehl ratio of ∼18 per cent were achieved.

The pre-explosion WFPC2 data were retrieved from the STScI archive,[9] and were processed with the most up-to-date calibration frames by the On-the-fly-re-calibration (OTFR) pipeline. The data were further processed, combined and photometry was conducted using the DOLPHOT package[10] (with the WFPC2 module). A further

[7] https://gelato.tng.iac.es/
[8] http://www.eso.org/sci/software/eclipse
[9] http://archive.stsci.edu/hst
[10] http://americano.dolphinsim.com/dolphot/ (version 2.0)

correction of −0.1 mag was applied to the WFPC2 photometry, to correct the photometry to an infinite aperture (Whitmore 1995).

The ACS Wide Field Channel (ACS/WFC) observations were also retrieved from the STScI *HST* data archive and processed through the OTFR pipeline. The ACS observations were composed of four separate dithered exposures. We considered two separate data products: the individual *FLT* distorted frames and the combined *DRC* frame, corrected for distortion and charge transfer inefficiency; photometry of these images was conducted using DOLPHOT (using the ACS module and the generic photometry mode, respectively). The distortion-corrected images have a pixel scale of 0.05 arcsec. The derived photometry was corrected to an infinite aperture using the tabulated corrections of Sirianni et al. (2005).

3.2 Results

Pre- and post-explosion images of the site of SN 2012ec are shown in Fig. 2. The geometric transformation between the post-explosion VLT/NACO image and pre-explosion WFPC2 images was calculated using 26 common stars, with a resulting rms uncertainty on the transformation of 0.017 arcsec. The transformed position of the SN is located on the PC chip. Two sources are recovered in the pre-explosion WFPC2 images in close proximity to the transformed SN position. Source A, the progenitor candidate, is detected in the WFPC2 *F814W* image only, offset from the transformed SN position by 0.030 arcsec with brightness $m_{F814W} = 23.39 \pm 0.18$ (detected at S/N = 5.9). The uncertainty on the astrometry for an object of the faintness of Source A is ∼0.020 arcsec (Dolphin 2000), such that the apparent discrepancy between the observed position of Source A and the transformed SN position is not significant. Source A is consistent with a point source with a measured sharpness value of −0.035 (good point-like sources should have sharpness values in the range −0.3 to 0.3). Source B is detected in the *F606W* and *F814W* images, offset from the SN position by 0.11 arcsec, with $m_{F606W} = 23.00 \pm 0.06$ and $m_{F814W} = 22.23 \pm 0.08$ mag. DOLPHOT claims a detection of Source B in the *F450W* image at $m_{F450W} = 24.15 \pm 0.18$, but on visual inspection of the image we suggest that this detection is questionable. Source A is absent from the pre-explosion WFPC2 *F606W* image; however, there is an extended source that overlaps with the SN position in the pre-explosion WFPC2 *F450W* image. It is unclear if any of the flux observed in the *F450W* image arises from Source A; given the scale of this feature, it is unlikely that all of the flux is due to Source A alone. Artificial star tests were used to derive the detection limit at the SN position in the pre-explosion WFPC2 *F450W* and *F606W* images, under the assumption that Source A does not contribute any flux in these images. We derived detection limits, corresponding to 50 per cent recovery efficiency at 3σ, of 24.5 ± 0.3 and 25 ± 0.5 mag in the *F450W* and *F606W* filters, respectively.

The geometric transformation between the post-explosion VLT/NACO image and the pre-explosion ACS/WFC *F814W* was derived using 25 common stars, with a resulting rms uncertainty of 0.016 arcsec. There is clear evidence for flux, above the background, at the transformed SN position, although DOLPHOT photometry of the distortion-corrected *DRC* image identifies the flux as being extended emission arising from Source B. Inspection of all four individual *FLT* images, however, revealed that this extended source is composed of two separate point sources, coincident with Sources A and B (the offset between the transformed SN position and Source A is 0.009 arcsec). We conclude that Source B is not an extended source and that the object observed in the ACS/WFC *DRC* images is a blend, arising from the MULTIDRIZZLE image combination process.
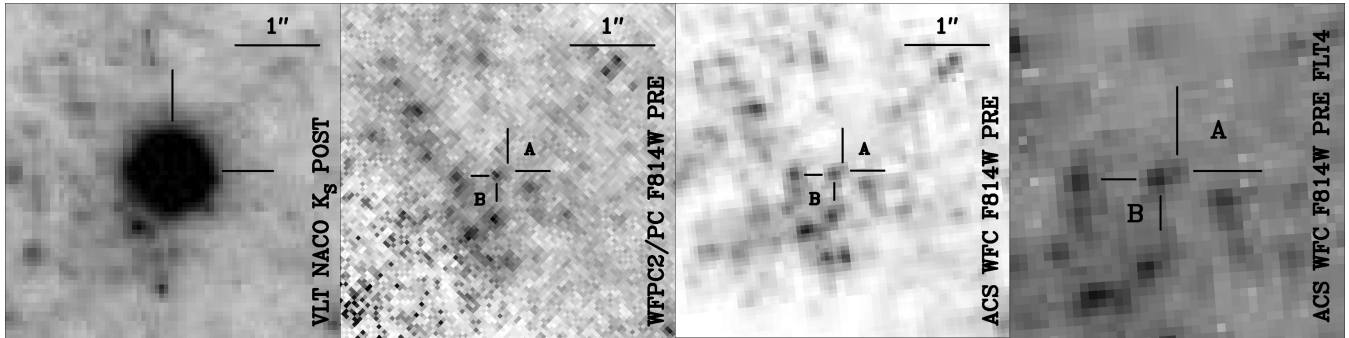
Figure 2. High spatial resolution observations of the site of SN 2012ec (all images are oriented such that North is up and East is to the left). From left to right: 4 arcsec × 4 arcsec VLT NACO post-explosion image stamp centred on SN 2012ec; pre-explosion *HST*/WFPC2/PC *F814W* image, with the positions of sources A and B marked by cross-hairs; pre-explosion *HST*/ACS WFC *F814W* image; and an ≈2 arcsec × 2 arcsec section of a *distorted* pre-explosion *HST*/ACS WFC *F814W* *FLT* image (data set jb4u02f0q_flt – note the pixels are not square on the sky) centred on Source A.

We measured the *F814W* magnitudes for the progenitor candidate (Source A) and Source B to be 23.10 ± 0.04 and 22.32 ± 0.02, respectively, averaged over the independent photometry of the four *FLT* images. Source A appears point-like in all four *FLT* images, with sharpness values of -0.072, -0.263, -0.075 and -0.064.

The brightness of Source B in the ACS/WFC *F814W* image is approximately consistent with the magnitude of Source B measured in pre-explosion WFPC2 *F814W* image. There is a discrepancy between the photometry of Source A in the ACS and WFPC2 *F814W* images, perhaps due to the difficulties in partitioning the flux between Sources A and B in the subsampled WFPC2 image (due to the relative faintness of Source A) and also the slight difference between the *F814W* filters used by the two instruments. Using synthetic photometry of MARCS spectral energy distributions (SED) (Gustafsson et al. 2008), we determined that, for the coolest red supergiants, the colour between the WFPC2 and ACS *F814W* filters is ~0.1 mag.

The observed photometry and upper limits for the progenitor candidate (Source A) were compared with the synthetic photometry of MARCS SED, using a Markov Chain Monte Carlo Bayesian infer-

ence scheme (Maund, in preparation). We considered the $15\,M_\odot$ spherical MARCS models, with the effective gravity fixed at $\log g = 0.0$ (Levesque et al. 2005), $\log Z/Z_\odot = +0.25$ and the reddening adopted in Section 2, assuming only foreground and host extinction following a Galactic-type $R_V = 3.1$ (Cardelli et al. 1989) reddening law. The corresponding allowed region on the Hertzsprung–Russell Diagram for the progenitor is shown in Fig. 3. The colour constraint provided by the pre-explosion *F606W* detection limit forces the resulting solution for the progenitor to cool temperatures consistent with a red supergiant ($<4000K$). The grid of comparison MARCS SED, however, only goes down to $3300K$ and lower temperatures, consistent with the end points of the twice solar metallicity stellar evolution tracks, cannot be probed. We determine a corresponding luminosity for the progenitor of $\log(L/L_\odot) = 5.15 \pm 0.19$. In comparison with the end points of solar and twice solar metallicity STARS stellar evolution tracks (Eldridge & Tout 2004), we infer an initial mass for the progenitor of 14–$22\,M_\odot$. If the progenitor is subject to additional reddening, by local dust destroyed in the SN, we can only constrain a lower initial mass limit of $14\,M_\odot$. In extrapolating the luminosity from the presented contours to lower
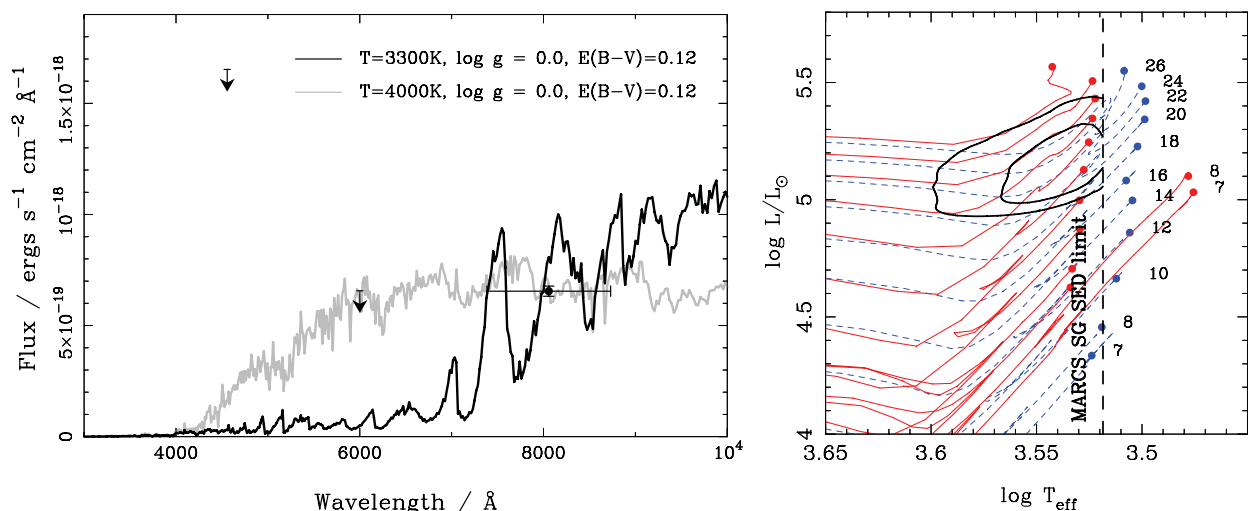

Figure 3. The photometric properties of the progenitor candidate for SN 2012ec. Left-hand panel: the observed SED of the progenitor candidate Source A (composed of detections and limits in the WFPC2 *F450W* and *F606W* and the ACS/WFC *F814W* bands) with MARCS spectra overlaid. The upper limits represent the 99 per cent-completeness limits derived from artificial star tests. Right-hand panel: the corresponding location of the progenitor candidate on the Hertzsprung–Russell diagram, the contours correspond to 68 and 95 per cent confidence intervals. Overlaid are STARS stellar evolution tracks for solar (red) and twice solar (blue) metallicities. The vertical dashed line corresponds to the lowest temperature of the grid of MARCS spectra.

temperatures, we expect that our derived mass estimate would not change significantly. The derived luminosity yields a radius for the progenitor of $R = 1030 \pm 180\,R_\odot$.

4 DISCUSSION AND CONCLUSIONS

We have presented the identification of the progenitor of a Type IIP SN, with an initial mass in the range 14–22 $M_\odot$. We have assumed that the extinction towards the progenitor is identical to the extinction affecting the SN. Walmswell & Eldridge (2012) and Kochanek, Khan & Dai (2012) explored the effect of dust formed in the winds of red supergiants, giving rise to additional extinction towards the observed progenitors of Type IIP SNe that is not probed by observations of surrounding stars or the SNe themselves (as this dust is destroyed in the subsequent explosion). Kochanek et al. (2012) showed that this dust may also have a significantly different composition and, hence, reddening law to the dust of the interstellar medium (Cardelli et al. 1989). In the case of the progenitor of SN 2012aw, which was detected at four different wavelengths (Fraser et al. 2012; Van Dyk et al. 2012), the constraints on the SED were insufficient to break the degeneracy between effective temperature and reddening. Fraser et al. (2012) found that the minimum reddening towards the progenitor of SN 2012aw was significantly larger than the reddening inferred towards the subsequent SN, suggesting that circumstellar dust around the progenitor was destroyed in the explosion. In the likely event that the progenitor of SN 2012ec suffers from greater extinction than inferred from post-explosion observations of the SN, our inferred mass range translates to a lower mass limit for the progenitor of $>14\,M_\odot$.

The lower end of the inferred mass range for the progenitor places it close to the maximum threshold observed for the red supergiant progenitors of Type IIP SNe (Smartt et al. 2009). Late-time observations of the site of SN 2012ec will be crucial to confirm the progenitor identification (through its disappearance) and its derived mass, and will be crucial to determine the nature of the extended emission observed in the pre-explosion WFPC2 *F450W* image (Maund & Smartt 2009).

Based on the early photometric and spectroscopic evolution of SN 2012ec, we conclude that it is a slightly brighter than average Type IIP SN. The similarities between the light curve and the spectroscopic evolution of SN 2012ec, with respect to early observations of other Type IIP SNe, suggest it was discovered only a few days (<6 d) post-explosion (Childress et al. 2012). Unlike the probable yellow supergiant progenitor of the Type II SN 2009kr ($M_{\rm ZAMS} = 15^{+5}_{-4}\,M_\odot$ – Fraser et al. 2010; 18–24 $M_\odot$ – Elias-Rosa et al. 2010), the apparent high mass of the progenitor of SN 2012ec indicates that stars at the maximum mass threshold ($\sim16\,M_\odot$) may explode as red supergiants and produce Type IIP rather than IIL SNe (Arcavi et al. 2012).

REFERENCES

Arcavi I. et al., 2012, ApJ, 756, L30
Asplund M., Grevesse N., Sauval A. J., Allende Prieto C., Kiselman D., 2004, A&A, 417, 751
Cappellaro E., Turatto M., 2001, Astrophysics and Space Science Library, Vol. 264, The Influence of Binaries on Stellar Population Studies. Kluwer Academic Publishers, Dordrecht, p. 199
Cardelli J. A., Clayton G. C., Mathis J. S., 1989, ApJ, 345, 245
Childress M., Scalzo R., Yuan F., Schmidt B., 2012, Cent. Bur. Electron. Telegrams, 3201, 2
Dolphin A. E., 2000, PASP, 112, 1383
Dopita M., Hart J., McGregor P., Oates P., Bloxham G., Jones D., 2007, Ap&SS, 310, 255
Eldridge J. J., Tout C. A., 2004, MNRAS, 353, 87
Elias-Rosa N. et al., 2010, ApJ, 714, L254
Elmhamdi A. et al., 2003, MNRAS, 338, 939
Fraser M. et al., 2010, ApJ, 714, L280
Fraser M. et al., 2012, ApJ, 759, L13
Gustafsson B., Edvardsson B., Eriksson K., Jørgensen U. G., Nordlund Å., Plez B., 2008, A&A, 486, 951
Hamuy M. et al., 2001, ApJ, 558, 615
Harutyunyan A. H. et al., 2008, A&A, 488, 383
Heger A., Fryer C. L., Woosley S. E., Langer N., Hartmann D. H., 2003, ApJ, 591, 288
King J. Y., Modjaz M., Shefler T., Halderson E., Li W. D., Treffers R. R., Filippenko A. V., 1998, IAU Circ., 6992, 1
Kochanek C. S., Khan R., Dai X., 2012, ApJ, 759, 20
Levesque E. M., Massey P., Olsen K. A. G., Plez B., Josselin E., Maeder A., Meynet G., 2005, ApJ, 628, 973
Li W., Cenko S. B., Filippenko A. V., 2009, Cent. Bur. Electron. Telegrams, 1656, 1
Li W. et al., 2011, MNRAS, 412, 1473
Maund J. R., Smartt S. J., 2009, Sci, 324, 486
Monard L., 2012, Cent. Bur. Electron. Telegrams, 3201, 1
Nakano S., Aoki M., Kushida Y., Kushida R., Benetti S., Turatto M., van de Steene G., 1996, IAU Circ., 6442, 1
Pastorello A. et al., 2006, MNRAS, 370, 1752
Pastorello A. et al., 2009, MNRAS, 394, 2266
Poznanski D., Prochaska J. X., Bloom J. S., 2012, MNRAS, 426, 1465
Quimby R. M., Wheeler J. C., Höflich P., Akerlof C. W., Brown P. J., Rykoff E. S., 2007, ApJ, 666, 1093
Ramya S., Sahu D. K., Prabhu T. P., 2007, MNRAS, 381, 511
Reichart D. et al., 2005, Nuovo Cimento C, 28, 767
Schlafly E. F., Finkbeiner D. P., 2011, ApJ, 737, 103
Sirianni M. et al., 2005, PASP, 117, 1049
Smartt S. J., 2009, ARA&A, 47, 63
Smartt S. J., Eldridge J. J., Crockett R. M., Maund J. R., 2009, MNRAS, 395, 1409
Tully R. B. et al., 2008, ApJ, 676, 184
Turatto M., Benetti S., Cappellaro E., 2003, in Hillebrandt W., Leibundgut B., eds, From Twilight to Highlight: The Physics of Supernovae. Springer-Verlag, Heidelberg, p. 200
Van Dyk S. et al., 2012, ApJ, 756, 131
Walmswell J. J., Eldridge J. J., 2012, MNRAS, 419, 2054
Whitmore B., 1995, in Koratkar A. P., Leitherer C., eds, Calibrating Hubble Space Telescope. Space Telescope Science Institute, Baltimore, MD, p. 269
Yaron O., Gal-Yam A., 2012, PASP, 124, 668

This paper has been typeset from a TEX/LATEX file prepared by the author.